

# Investigation of a measurement technique to estimate concentration and size of inclusions in droplets

Norbert Riefler<sup>1</sup>, Roman Schuh<sup>1</sup> and Thomas Wriedt<sup>2</sup>

<sup>1</sup> Universität Bremen, FB4, Verfahrenstechnik, Badgasteiner Strasse 3, 28359 Bremen, Germany

<sup>2</sup> Stiftung Institut für Werkstofftechnik, Badgasteiner Strasse 3, 28359 Bremen, Germany

E-mail: [riefler@iwt.uni-bremen.de](mailto:riefler@iwt.uni-bremen.de)

Received 19 February 2007, in final form 10 April 2007

Published 19 June 2007

Online at [stacks.iop.org/MST/18/2209](http://stacks.iop.org/MST/18/2209)

## Abstract

Inhomogeneous droplets including small spherical inclusions are characterized by the estimation of droplet diameter, inclusion concentration and inclusion diameter and a measure for the polydispersity of the inclusions. In most cases, it is reasonable to assume that the material parameters are known and therefore the index of refraction and the shape of inclusions. In this paper, the results from a measurement technique are investigated. The method will be evaluated on the basis of light scattering measurements for a range of scattering angles. These measurements have been taken with a fast CCD line scan camera and appropriate optics. An attempt is made to derive information from these measurements only. The continuous wavelet transform, speckle image analysis and turbidity measurement methods are used to estimate the concentration and the diameter of the monodisperse polystyrene particles within a droplet. The droplets, generated by a drop-on-demand droplet generator, are nearly monodisperse. The volume concentration of the inclusions within the suspensions varies between 0.01% and 9%. The inclusions are monodisperse. However, it seems to be possible that they coagulate due to the fast fluid flows at the droplet generation. As a result, the technique may be used only for the estimation of average values of size and concentration of inclusions from the measurements.

**Keywords:** inclusion size and concentration, inhomogeneous droplets, speckle image analysis, turbidity measurements, wavelet transform, static light scattering

(Some figures in this article are in colour only in the electronic version)

## 1. Introduction

Fluid droplets with small inclusions are common in medicine, environmental research and industry. The diameter range of the host droplets usually is between 10 and 1000  $\mu\text{m}$  whereas the inclusions are much smaller, usually from some microns down to some nanometres. For instance, cough droplets include pathogenic bacteria or viruses, atmospheric water droplets contain inclusions like soot, and in spray drying

techniques, inhomogeneous liquids are dispersed in order to manufacture industrial products such as instant coffee.

In all these examples, information is desired about the size of the host droplets and their inclusions together with the concentration of the inclusions. This can be done non-invasively with optical measurement systems. In principle these systems use the extinction or the scattering of light caused by the object. Extinction measured by turbidity measurements gives insufficient characterization of droplets with inclusions.

More information about these particles can be obtained by measuring systems using scattered light because of its complex and rich structure.

Depending on the size and concentration of the inclusions, the resulting scattering patterns are more or less like those of a pure ‘Mie’ particle when using laser light illumination. With a higher number of inclusions, that part of the scattered light originating from multiple scattering increases. Without inclusions the scattered light shows typical Mie fringes on a diffusing screen. However, in the case of a droplet with many inclusions, one can observe typical speckle patterns.

Droplets with a single inclusion are experimentally treated by Krieger *et al* [1] and theoretically by Videen *et al* [2, 3] and by Gouesbet *et al* [4]. A video demonstration could be viewed from Prabhu *et al* [5] showing the scattering patterns depending on the size and position of the inclusion.

The experimental setup for the acquisition of scattering patterns is frequently based on electrodynamic trapping of host droplets (e.g., Bronk *et al* [6], Videen *et al* [7], Krieger *et al* [1], Jakubczyk *et al* [8]). Bronk *et al* [6] and Videen *et al* [7] used dynamic light scattering (DLS) to analyse levitated droplets with inclusions. However, both studies sum up that the DLS method produces wrong results. Jakubczyk *et al* [8] studied light scattering of evaporating levitated droplets with inclusions. They deduced a modified Lorentz–Lorenz effective medium formula from investigations of the light-scattering intensity patterns. This formulation allows the estimation of the filling factor and of the volume of the inclusions. The background for their application of effective medium theory was to overcome the difficulties with levitated droplets. Because electrodynamic levitation causes high frequency, random vibration and rotation of the droplets, it is very difficult to measure the Brownian motion of the inclusions.

This drawback does not occur when using a piezoelectric droplet generator which can be used to produce monodisperse droplets with inclusions. Unfortunately, DLS measurements are not possible because of the far too short time of interaction of a moving droplet (velocity  $v \sim 2 \text{ m s}^{-1}$ ) with the laser beam within the measurement volume. Instead of DLS, phase Doppler anemometry (PDA) can be used for an optical characterization of droplets with inclusions if the size distribution is narrow and the concentration of the individual droplets differs only slightly. Onofri *et al* [9] estimate the size and the velocity of the cylindrical jets together with the concentration of the inclusions by using PDA. A modified PDA method using a CCD line scan camera is described by Rheims *et al* [10]. These authors used a differential (i.e. angle resolved) PDA to measure the diameter of droplets generated by a droplet generator. Wriedt *et al* [11] also used a CCD line scan camera. However, they analysed the static light scattering response instead of using a PDA method to get information about droplets from a droplet generator. Their method can be used to estimate the concentration of the inclusions if all inclusions have the same size.

In this paper, we describe an optical measurement method to estimate the concentration as well as the size of the inclusions. We use a piezo drop-on-demand droplet generator to produce monodisperse droplets and examine the light scattering intensities of a droplet from different scattering

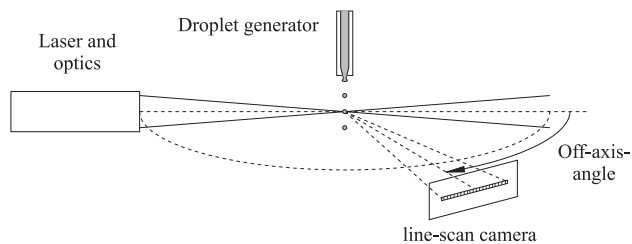


**Figure 1.** Experimental setup: a weakly focused argon-ion laser beam illuminates droplets from a droplet generator; the light scattered from the droplets will be detected from a CCD line-scan camera within a range of angles of  $27^\circ \leq \theta \leq 46^\circ$ .

angles using a fast CCD line scan camera. From the information from static light scattering we get additional information about the dynamic property of the inclusions by means of capturing consecutive scattering data with a sampling frequency of about  $f_s \simeq 79 \text{ kHz}$ . Because water is commonly used as a host fluid and polystyrene is a very common material with well-defined characteristics for modelling in science and industry, we have chosen water for the host droplets and polystyrene for the inclusions.

In the next section, we will give an outline of the measuring system and then describe the data analysis methods. First of all, the measured data will be filtered to suppress the oscillations coming from the Mie scattering of the host droplet. The filtered data ensure that the following evaluation routines yield usable and comparable results.

To estimate the inclusion concentration, we will use the continuous wavelet transform (CWT) rather than the orthogonal discrete wavelet transform (DWT) because the CWT is more suitable to detect structures than the DWT.

For the estimation of the inclusion size, we will do a speckle analysis of each captured CCD line including the light scattering data at a time point. To get a reasonably unique correspondence between the estimated values—from CWT as well as speckle analysis—and the real values (diameter and concentration of the inclusions), we additionally include turbidity measurements in our evaluation.

Finally, we will present exemplary measurement results analysed by the described analysis method. The method for the estimation of the concentration and diameter of the inclusions within a host droplet is verified on the basis of the given particle parameters. Together with the work on sizing droplets with inclusions (Schuh *et al* [12]), we are able to get the most essential information about droplets with inclusions.

## 2. Experimental setup

In this section, we will give a short description of the measurement setup which we will use in our experiments. The light source is a continuous wave argon-ion laser ( $\lambda = 514.5 \text{ nm}$ ,  $800 \text{ mW}$ ). The beam is weakly focused on the trajectory of the droplets. The piezoelectric droplet generator (figure 1) generates monodisperse droplets on demand within the range of  $20\text{--}100 \mu\text{m}$  at a selectable frequency of less than about  $10 \text{ kHz}$  [13]. The light scattered from the droplets is collected at a distance of  $80 \text{ mm}$  with a lens system and detected with a CCD line-scan camera (Dalsa,  $512 \text{ pixels}$ ,

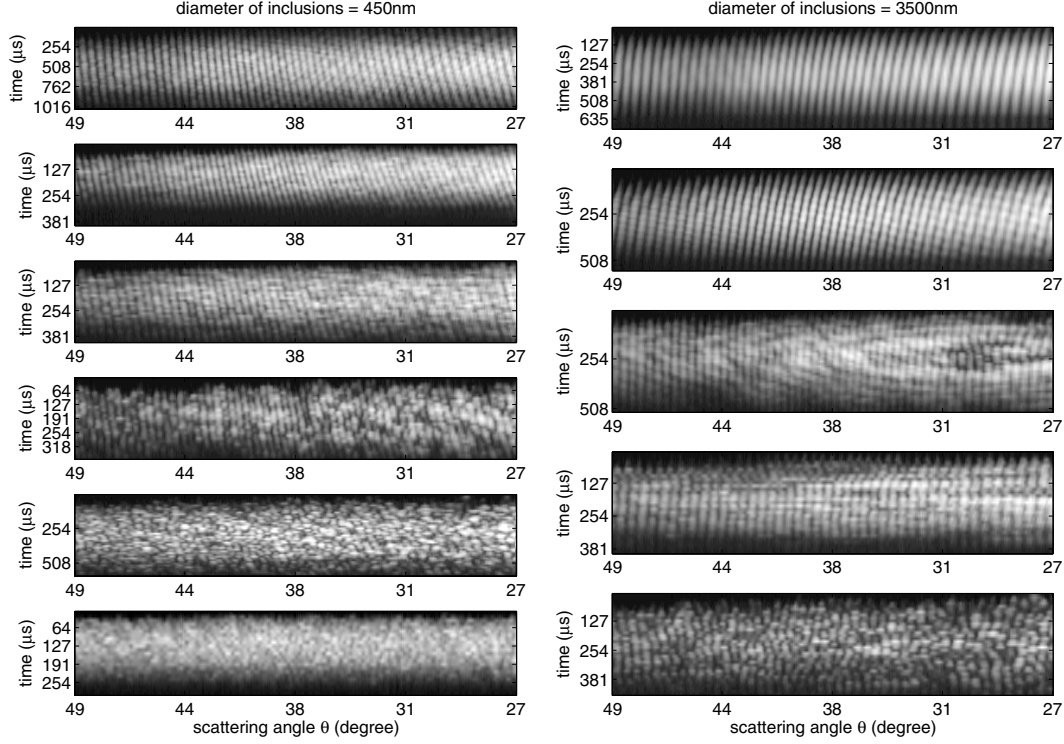


**Figure 2.** Examples of measurements of droplets with inclusions which have all the same diameter of 450 nm (left side) and 3500 nm (right side) but different concentrations; each picture corresponds to one droplet with individual diameter; the volume concentration increases from top to bottom: (left side)  $c = 0.01\%$ ,  $0.03\%$ ,  $0.1\%$ ,  $0.3\%$ ,  $1\%$  and  $3\%$  and (right side)  $c = 0.1\%$ ,  $0.3\%$ ,  $1\%$ ,  $3\%$  and  $7\%$ .

**Table 1.** Mean diameter and standard deviation of the automated diameter determination.

	$d_{\text{incl}} = 450 \text{ nm}$	$d_{\text{incl}} = 720 \text{ nm}$	$d_{\text{incl}} = 1400 \text{ nm}$	$d_{\text{incl}} = 3500 \text{ nm}$
$c_V = 0.01\%$	$91.3 \pm 1.1 \mu\text{m}$			
$c_V = 0.03\%$	$103.0 \pm 0.4 \mu\text{m}$			$76.1 \pm 2.6 \mu\text{m}$
$c_V = 0.1\%$	$84.9 \pm 1.5 \mu\text{m}$		$71.9 \pm 3.6 \mu\text{m}$	$78.5 \pm 2.5 \mu\text{m}$
$c_V = 0.3\%$	$95.6 \pm 1.1 \mu\text{m}$	$72.5 \pm 1.2 \mu\text{m}$	$67.1 \pm 0.9 \mu\text{m}$	$88.0 \pm 1.4 \mu\text{m}$
$c_V = 1\%$	$89.4 \pm 1.2 \mu\text{m}$	$76.1 \pm 0.8 \mu\text{m}$	$68.1 \pm 1.0 \mu\text{m}$	$69.5 \pm 0.8 \mu\text{m}$
$c_V = 3\%$	$102.1 \pm 2.0 \mu\text{m}$	$71.0 \pm 0.9 \mu\text{m}$	$66.4 \pm 1.0 \mu\text{m}$	$75.8 \pm 1.0 \mu\text{m}$
$c_V = 7\%$		$71.4 \pm 0.9 \mu\text{m}$	$78.5 \pm 6.6 \mu\text{m}$	$91.6 \pm 1.5 \mu\text{m}$
$c_V = 9\%$	$98.6 \pm 2.2 \mu\text{m}$			

resolution 8 bits, line sampling rate  $f_s = 79 \text{ kHz}$ ). In our configuration, the scattering range covered by the camera is  $27^\circ \leq \theta \leq 49^\circ$ . We want to call each line of a frame a scattering diagram.

We use distilled and microfiltered water and add monodisperse spherical polystyrene particles (PS) with diameters  $d_{\text{incl}}$  of 450 nm, 720 nm, 1400 nm or 3500 nm, produced in our laboratory. The concentration varies between 0.01% and 9% volume concentration. For every diameter and concentration of PS inclusions, 100 measurements are saved in computer files. Examples of typical measurements are shown in figure 2. These measurements are represented as frames. Each frame corresponds to the measurement of one droplet.

The droplets are thermodynamically stable. The rate of change of droplet diameter with time caused by evaporation is [14]

$$\frac{dr}{dt} = -\frac{\beta_v}{2r}. \quad (1)$$

With an evaporation coefficient  $\beta_v = 6.44 \mu\text{m}^2\text{s}^{-1}$ , the decrease of droplet radius will be  $dr = -0.73 \mu\text{m}$  after 10 s.

At first glance, there is a shift of the brightest part of the frame from the right (low scattering angles) to the left (higher scattering angles) for increasing concentrations. This effect is based on the increasing number of inclusions, which all contribute to the diffuse scattering in all directions. In contrast, a droplet with less inclusions scatters more light in the forward direction. At very dilute concentrations, the droplet corresponds to a Mie scatterer. This observation is used to estimate the concentration of the inclusions in the work presented here as well as in a former work [11].

In addition, the diameters of the droplets are measured with an optical microscope. However, we found that the estimation of the droplet diameter using a spatial frequency analysis of the measured scattering pattern described in [12] yields better values than the optical estimation. The measured diameter of the droplets vary slightly within the 100 measurements which belong to one PS diameter and concentration (see table 1). In contrast, the droplet diameters of different measurement series vary between  $66 \mu\text{m}$  and  $102 \mu\text{m}$ .

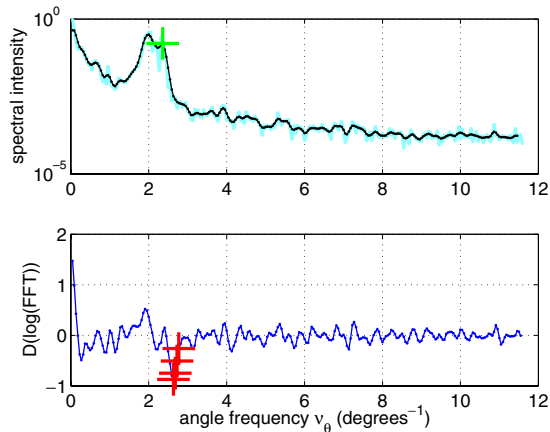


**Figure 3.** Top figure: Fourier transformed signal (bright (blue) line: unfiltered, black line: low-pass filtered) together with the resulting angle frequency (cross); lower figure: differential of the low-pass filtered signal with three sequential points (crosses) all fulfilling the consecutive criterion.

### 3. Data analysis

The first trial to estimate correct values of the inclusion size and concentration from the raw measurement data failed. We needed to preprocess the data. The procedure used contains the estimation of the droplet diameter and a subsequent filtering of the data. The measured data will be filtered by the scattering response of a pure droplet without inclusions, which will be calculated by a Mie program using the host droplet diameter. Therefore, the most important step for the filtering is, as far as possible, an exact estimation of the droplet diameter whose estimation principle will be described fully in [12]. We will filter each measurement line-by-line for further data processing.

The filtered data will then be evaluated by three independent methods: wavelet, turbidity and speckle analysis. The last two methods will be combined to yield one specific parameter which corresponds to the size of the inclusions. This parameter will be combined with the parameter of the wavelet method, which corresponds to the concentration of the inclusions. In the end, we will get two parameters to graphically determine the size and the concentration of the inclusions.

#### 3.1. Mie filtering

The first step to filter out the scattering of the pure droplet is to estimate the diameter of each individual droplet. Schuh *et al* [12] describe a procedure using the Fourier transform to find the angle frequency where the transformed signal shows a deep fall down. At this exact point, the angle frequency corresponds to the spatial end of the droplet or, in other words, this angle frequency corresponds to the diameter of the droplet. Please refer to [12] for more detailed information.

For an analysis of thousands of measurements, we developed an algorithm to find the steep slowing down of the curve via a low-pass filtering of the Fourier transformed signal and a following differentiation, an example of which is represented by figure 3. To accomplish this the algorithm

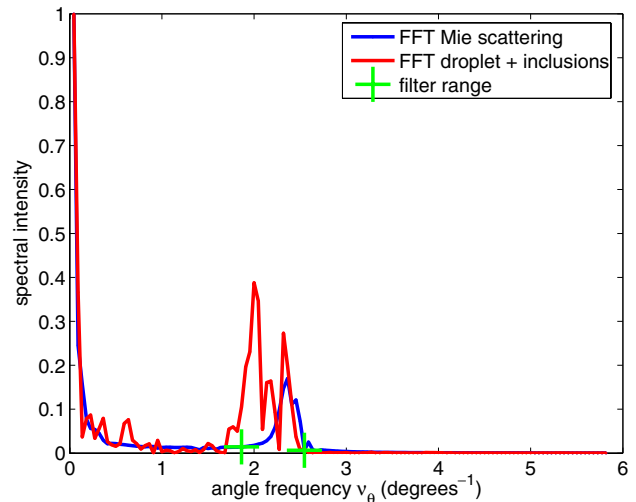


**Figure 4.** Pure droplet (dark (blue) line) and droplet with inclusions (bright (red) line); the filter range is indicated with the two crosses.

evaluates the first-order differential of the low-pass filtered Fourier transformed signal. The criterion for the desired angle frequency is to find at least five consecutive gradient values of the differential where all of them have a slope greater than an empirical specified value (in our case of logarithmic values  $d(\log F)/dx < -0.1$ ). This is demonstrated in figure 3. The data are from a droplet with inclusions having a volume concentration  $c_V = 0.1\%$  and diameter  $d_{\text{incl}} = 3.5 \mu\text{m}$ . The results of the automated diameter determination are shown in table 1.

The resulting droplet diameter will be entered into a subroutine to calculate the Mie scattering which again will be Fourier transformed. With a method similar to the one described above consecutive points are extracted from the pure Mie scattering to find a band-pass filter range of the signal which belongs to the pure droplet. This filter range will be subtracted from the Fourier transformed measured scattering data. A sketch of this method can be seen in figure 4.

The position of the upper angle frequency in figure 4 (right cross) is not particularly important, but the lower frequency (left cross) has to be adjusted carefully to avoid both the truncation of the desired signal from the inclusions as well as the remaining of too much of the frequency spectrum from the pure droplet in the filtered signal. The lower frequency is estimated empirically. Using a too small value filters out the scattering of the inclusions, while a too high value leads to the remaining of the scattering of the pure droplet. We adjusted the lower frequency as a compromise between these two effects.

The Mie filtered signal should now consist essentially of the scattering response only from the inclusions. Because of the multiple scattering between host droplet and inclusions, the scattering of the pure droplet and that of the inclusions cannot be divided completely. However, the frequency range of the scattering response is different so there is at least a strong suppression of the signal from the pure droplet. The filtering effect can be seen in figure 5. The measured data (top) show the typical oscillations from the Mie scattering which are in the form of vertical stripes. In the Mie filtered data (below), these

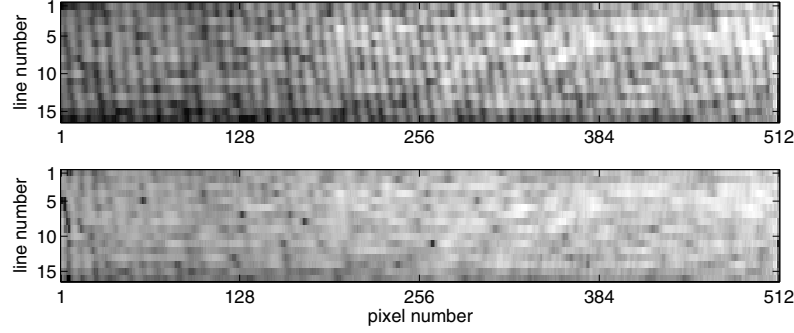


**Figure 5.** Original (top) and filtered image of a measurement;  $d_{\text{host}} = 97.3 \mu\text{m}$ ,  $d_{\text{incl}} = 450 \text{ nm}$ ,  $c_{\text{incl}} = 0.1\%$ .

stripes have nearly disappeared. Attention should be paid to the unit of the  $x$ -axis (pixel number), which corresponds to the scattering angle, and the unit of the  $y$ -axis (line number), which corresponds to the time. Please see figure 2 for physical units.

### 3.2. Concentration analysis

We used the continuous wavelet transform (CWT) for analysing the measured light scattering signals. We did not get useful results using the discrete wavelet transform (DWT). In general, the CWT has some advantages compared to the DWT especially in data analysis or image recognition [15]. The continuous wavelet transform  $\tilde{f}(s, t)$  of a signal  $f(u)$  ( $u$  may be the time parameter) is defined by [16]

$$\tilde{f}(s, t) = \int_{-\infty}^{\infty} \psi_{s,t}(u) f(u) du, \quad (2)$$

where  $\psi_{s,t}(u)$  is the wavelet function (mother wavelet):

$$\psi_{s,t}(u) = \psi_s(u - t) = |s|^{-1/2} \psi\left(\frac{u - t}{s}\right) \quad (3)$$

with  $s \in \mathbb{R} \setminus \{0\}$  as the scale (or dilation) and  $t \in \mathbb{R}$  as the translation parameter, sometimes called the position parameter. In our case,  $t$  is related to the scattering angle  $\theta$ . For each pair of  $s$  and  $t$ ,  $\tilde{f}(s, t)$  is a coefficient which reproduces the similarity of the scaled and dilated wavelet about  $s$  and  $t$ ,  $\psi_{s,t}$ , to the signal  $f(u)$ .

The wavelet transform produces one spectrum of scales  $s$  at each scattering angle  $t$ . To relate these scalograms to the real concentrations of inclusions in the droplets, we calculated the centre-of-mass  $x_m$  from the 2-dimensional scalogram of the CWT for one line of all 512 pixels, i.e. scattering angles [17, 18]:

$$x_m = \frac{m_{10}}{m_{00}}. \quad (4)$$

The moments  $m_{kl}$  are defined by

$$m_{kl} = \sum_{x,y} x^k y^l b(x, y) \quad (5)$$

where  $b(x, y)$  is the brightness of a point of the image. In our case, the image is a scalogram and  $b(x, y)$  corresponds to the wavelet coefficient  $\tilde{f}(s, t)$ , so the discrete coordinates  $x$  and  $y$  correspond to  $s$  and  $t$  (i.e. scattering angles) of the scalogram. The quantity  $m_{00}$  is recognized as the average

brightness of the complete scalogram and  $m_{10}$  is the average brightness according to the  $x$ -direction.

For the analysis of the measurements with the centre-of-mass formulation, we will take the brightest line (BL) of one measurement (i.e. every frame in figure 2). After a CWT of the BL we will get a scalogram and therefore we will calculate  $x_m$ . Because we want to know if  $x_m$  obtained from the BL is really representative, we repeat this procedure for the other lines of a measurement and calculate the mean value of  $x_m$ . This one number represents the measurement concerning the concentration of the inclusions.

We find that the Gaussian wavelet is the most suitable wavelet family for the measured signals. The Gaussian wavelets are defined as derivatives of the Gaussian probability density function:

$$\psi(u) = c_n \frac{d^n e^{-u^2}}{du^n}, \quad (6)$$

where  $c_n$  is the scale factor. The Gaussian wavelet with the second derivative is closely related to the Marr and the Mexican hat wavelet.

### 3.3. Turbidity

The turbidity  $\tau$  of a droplet with inclusions illuminated by a single wavelength is given by [19]

$$\tau = \frac{1}{l} \ln \left( \frac{I_0}{I} \right) \quad (7)$$

with the geometric length of the sample  $l$ , the intensity of the light source  $I_0$  and the measured intensity  $I$ . This equation is the rearranged well-known exponential Lambert–Beer law. In common turbidimetric measurements,  $I$  is measured under one scattering angle (usually  $\theta = 90^\circ$  for nephelometers), whereas  $I_0$  is known by a light source monitor detector. However, turbidimetric measurements are also taken under different scattering angles [19]. In the case of our measurements, the intensity of the laser used in our experiments cannot be assumed to be constant during all measurements. Therefore, we estimate a representative value of  $I_0$  from every measurement.  $I$  and  $I_0$  are estimated by a detector integration of the values from the CCD line-scan sensor:

$$I = \int_0^{2\pi} \int_{\theta_{\min}}^{\theta_{\max}} I(\varphi, \theta) \sin \theta d\theta d\varphi \quad (8)$$

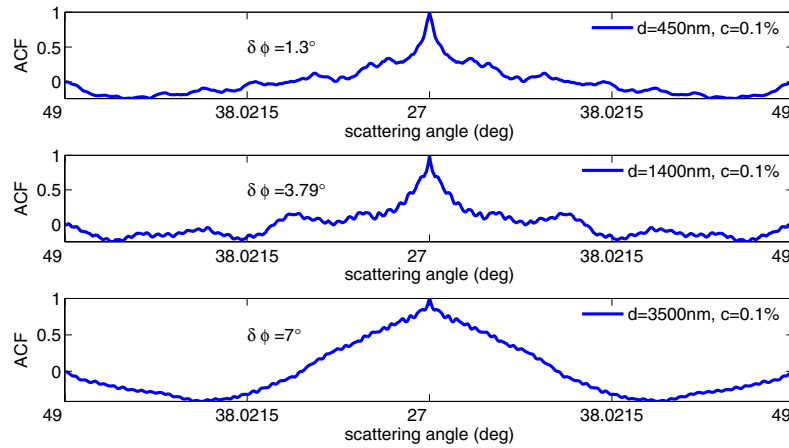


**Figure 6.** Autocovariance function of measured scattering diagrams for three different inclusion diameters  $d_{\text{incl}} = 450, 1400$  and  $3500$  nm and one inclusion concentration  $c_V = 0.1\%$ ; the FWHM values of the angle are  $\delta\phi = 1.3^\circ$ ,  $\delta\phi = 3.79^\circ$  and  $\delta\phi = 7.0^\circ$  which correspond to  $d_{\text{incl}} = 532, 1903$  and  $3583$  nm using equation (10).

with the upper and lower scattering angles  $\theta_{\min}$  and  $\theta_{\max}$ .  $I_0$  is determined over the complete measured range of scattering angles  $\theta_{\min} = 27^\circ$  and  $\theta_{\max} = 49^\circ$  from the raw, unfiltered measurement values. The intensity  $I$  is determined by the integration of  $\theta_{\min} = 27^\circ$  and  $\theta_{\max} = 28^\circ$ . Both  $I_0$  and  $I$  are estimated using equation (8) for every line of a measurement (see figure 2). Then, the ratio  $I/I_0$  of each line is averaged over all lines to give the scattered brightness ratio of every measurement. The standard deviation of  $I/I_0$  for the different suspensions is below 5%.

### 3.4. Speckle analysis

Speckles are stochastic optical signals under coherent illumination. In figure 2, the lowermost frame on the left shows a typical speckle pattern. An application of speckle analysis is the measurement of the 2-dimensional surface roughness of an object. However, it is also possible to measure a 3-dimensional random distribution of particles [20]. The mean speckle size corresponds to the full-width-half-maximum (FWHM) value of the autocovariance (ACF) function at a discrete point  $m$ :

$$ACF(m) = E[(x_n - \mu_x)(x_{n+m} - \mu_x)] \quad (9)$$

with the discrete value of the stochastic variable  $x_n$ , the mean value of the stochastic process  $x$ ,  $\mu_x$ , and  $E[\dots]$  is the expected value operator. Examples of autocovariance functions resulting from evaluations of measured scattering diagrams can be seen in figure 6. Because the FWHM value corresponds to the speckle size of scattering diagrams, we denote the result with  $\delta\phi$ . The relation of  $\delta\phi$  to the diameter of the scatterers, i.e. the inclusions,  $d_{\text{incl}}$  is established by the formula of the first diffraction minimum  $\delta x = 1.22\lambda z/d$  with the distance  $z$  between the scattering object and the observation plane and the factor 1.22 as the first zero of the first Bessel function. In terms of the angular diameter, the previous relation is equivalent to

$$\delta\phi = \left( \arctan \frac{\lambda}{d_{\text{incl}}} \right)^{-1}. \quad (10)$$

Results for  $d_{\text{incl}}$  are given in figure 6. It should be mentioned that the results from equation (10) depend additionally on the concentration of the inclusions (e.g. in figure 10).

## 4. Results

All the droplets from the droplet generator have nearly the same diameter and velocity within the 100 measured frames for each set of inclusion diameter and concentration. However, velocities and diameters differ between different pairs of inclusion diameters and concentrations. Hence, the residence time of the droplet within the measuring volume is different so the number of measured lines varies between 20 and 50 lines. Therefore, we use only 16 lines for all evaluations to ensure identical conditions for each of them. In this work, we do not take into account the different velocities of the droplets.

### 4.1. Concentration analysis

The first step in concentration analysis is the wavelet transform of one line of the measured intensities. We chose discrete scales  $s = 1, \dots, 64$ . Each point in the scalogram corresponds to the coefficient of the wavelet transform. The centre-of-mass  $x_m$  enables us to relate the scalograms to the concentration of the droplets from the measurements. The observed property in section 2 can be stated as follows: the higher the concentration the larger the left shift of the centre of mass. This can be seen in figures 7 and 8, where the bright areas, which correspond to high values of the wavelet coefficients, shift to the right for decreasing concentrations. The scalograms of one row have the same concentration of inclusions with diameters of 450 nm and 3500 nm, respectively. Each scalogram is related to one value of the centre-of-mass  $x_m$  in tables 2 and 3.

The values of the centre of mass in table 2 do not at all increase continuously with decreasing concentration. However, evaluation of all lines of one measured picture instead of using only the brightest line results in continuously increasing values. We show this by means of droplets with inclusions having a diameter of  $d = 1400$  nm. Again, table 4 looks rather unsorted, whereas in table 5, all lines are averaged instead of using only the brightest line as in table 4.

An interesting observation needs to be mentioned here. The ‘left-shift’ property from above seems to be violated sometimes. For example, some of the scalograms in figure 8 for inclusions with a diameter of  $d = 3500$  nm but different

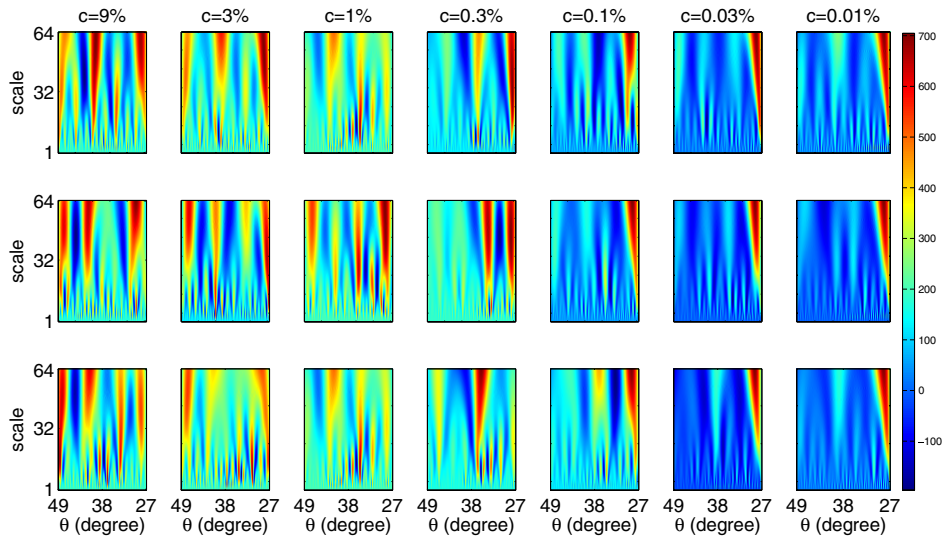


**Figure 7.** Scalograms of droplets with inclusions of diameter  $d = 450$  nm; each scalogram was calculated from one measured scattering diagram; (from top to bottom) different droplets having the same inclusion concentration; (from left to right) the inclusion concentrations are in descending order; each of these scalograms are related via the centre-of-mass  $x_m$  to the scattering angle from table 2.

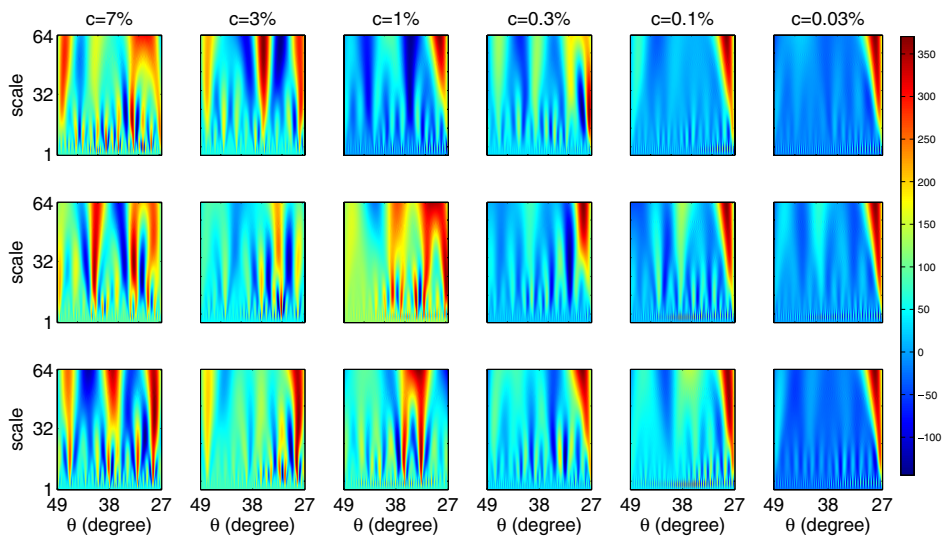


**Figure 8.** Scalograms of droplets with inclusions of diameter  $d = 3500$  nm; each scalogram was calculated from one measured scattering diagram; (from top to bottom) the droplets have the same inclusion concentration; (from left to right) the inclusion concentrations are in descending order; each of these scalograms is related via the centre-of-mass  $x_m$  to the scattering angle from table 3:

**Table 2.** Centre of mass of the scalograms from figure 7.

$c$	9%	3%	1%	0.3%	0.1%	0.03%	0.01%
$x_m$	38.5	34.0	32.6	32.6	32.6	34.0	36.9
$x_m$	35.8	34.2	34.4	34.4	34.4	34.2	35.0
$x_m$	38.0	31.1	29.1	29.1	29.1	31.1	37.1

**Table 3.** Centre of mass of the scalograms from figure 8.

$c$	7%	3%	1%	0.3%	0.1%	0.03%
$x_m$	35.5	31.5	29.3	29.3	29.3	31.5
$x_m$	37.2	31.5	30.4	30.4	30.4	31.5
$x_m$	36.6	30.4	29.8	29.8	29.8	30.4

concentrations look similar, although they belong to droplets with different inclusion concentrations. We assume that there are two reasons for this violation.

First, an estimation of the number density of inclusions within a droplet shows that for a volume concentration of  $c = 1\%$  there are about  $n = 119$  inclusions in a host droplet

with about  $d = 80 \mu\text{m}$ . However, for the concentration  $c = 0.03\%$  the rounded number of inclusions is only  $n = 4$ . In the case of such a small number of inclusions, we assume that the similarities in the scalograms of different concentrations are caused by the statistical fluctuation in the number of inclusions.

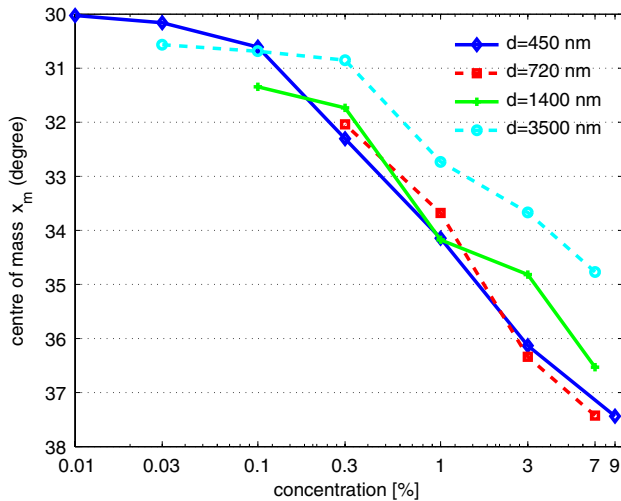


**Figure 9.** Each curve corresponds to one inclusion diameter and shows the scattering angle of the centre-of-mass  $x_m$  as a function of the logarithmic values of concentrations  $c$ .

**Table 4.** Centre of mass for scalograms from droplets with inclusion diameter  $d = 1400$  nm, using only the brightest line.

$c$	7%	3%	1%	0.3%	0.1%
$x_m$	36.9	40.1	32.6	32.6	32.6
$x_m$	36.3	33.3	32.1	32.1	32.1
$x_m$	36.0	34.1	30.4	30.4	30.4

**Table 5.** Centre of mass averaged over all lines.

$c$	7%	3%	1%	0.3%	0.1%
$x_m$	37.0	35.3	31.6	31.6	31.6
$x_m$	36.1	33.0	31.6	31.6	31.6
$x_m$	37.9	34.9	31.9	31.9	31.9

Second, the deviations of  $x_m$  derived from the brightest line (BL) for droplets with bigger inclusions are higher than for the droplets with smaller inclusions. We compare the result for the centre-of-mass  $x_m$  of one BL with the mean value of all lines (AL) of the same measurement. The deviation of  $x_m$  between the analysis of one BL and the mean value of ALs is usually smaller than  $\Delta\theta = 0.8^\circ$ . Therefore, it is possible to relate the concentration and the scalogram of only the brightest line. This saves a lot of computing time.

In figure 9, the semilogarithmic plot of the averaged centre-of-mass scattering angle values against the logarithmic concentrations shows nearly straight lines for concentrations above 0.3%. However, it is not possible to determine the concentration of inclusions within an individual droplet from the centre of mass even if the diameter of inclusion is known because the standard deviation of the 100 measurements is very high. Because the error bars would disturb the figure, we include the standard deviation in table 6.

#### 4.2. Inclusion diameter analysis

The method for the estimation of the concentration is until now ambiguous. The value of the centre of mass from a measurement can be related to more than one concentration,

**Table 6.** Mean values and standard deviations from the CWT analysis (figure 9); blank fields indicate that for those inclusion diameters and concentration pairs no measurements are performed.

$d$	450 nm	720 nm	1400 nm	3500 nm
$c = 9\%$	$37.4 \pm 1.6$			
$c = 7\%$		$37.4 \pm 1.7$	$36.5 \pm 1.7$	$34.8 \pm 1.0$
$c = 3\%$	$36.1 \pm 1.2$	$36.3 \pm 1.3$	$34.8 \pm 2.5$	$33.7 \pm 3.1$
$c = 1\%$	$34.1 \pm 2.6$	$33.7 \pm 1.5$	$34.2 \pm 4.8$	$32.7 \pm 3.1$
$c = 0.3\%$	$32.3 \pm 2.3$	$32.0 \pm 2.0$	$31.7 \pm 2.7$	$30.9 \pm 0.3$
$c = 0.1\%$	$30.6 \pm 1.3$		$31.3 \pm 4.4$	$30.7 \pm 0.1$
$c = 0.03\%$	$30.2 \pm 1.7$			$30.6 \pm 0.2$
$c = 0.01\%$	$30.0 \pm 0.2$			

depending on the size of inclusions. However, with the inclusion size analysis we get a second value for the two unknown parameters: *concentration* and *inclusion size*.

The estimation procedure begins with the calculation of the ACF (equation (9)) of every 16 evaluated lines. Averaging of the FWHM yields the  $\delta\phi$ -value which is representative of one measurement. The final results of all measured data are depicted in figure 10. We did not insert error bars with the standard deviation of the averaged measurements in this figure because the variances are very high and the error bars would disturb the figure. Hence we present numerical values of the standard deviations in table 7. The high standard deviations indicate that one only gets measurement results which are based on averaged values of many droplets. Below we will emphasize that the polystyrene particles are likely coagulated to a large part.

#### 4.3. Combination of methods

We will now bring together the three methods of analysis. We will get two values from one measured picture:

- a centre-of-mass value  $x_m$  from the wavelet analysis,
- a value of the speckle size, weighted by the intensity ratio  $I/I_0$ .

The averaged results of all measurements are represented in two different manners. The curves of the left part in figure 11 represent the results which are arranged in order of diameter. The curves of the right part are arranged in order of concentration. Straight lines are additionally inserted there which depict a simple fit of those results having the same concentration.

## 5. Discussion

The results shown in figure 11 are not unique: first, the large standard deviations lead to overlaps of the determined values for different inclusion parameters; and second, the curves sometimes intersect each other. Thus, it is important to discuss some possible reasons for the non-uniqueness of the results.

The evaluation of only 100 measurements for one pair of inclusion diameter and concentration is a statistically small number in respect of the many physical parameters which influence the state of a droplet with inclusions. To begin with, an important physical effect is the flocculation or coagulation of the PS particles. Each pair of particles within a fluid is subject to attractive van der Waals forces. On the other

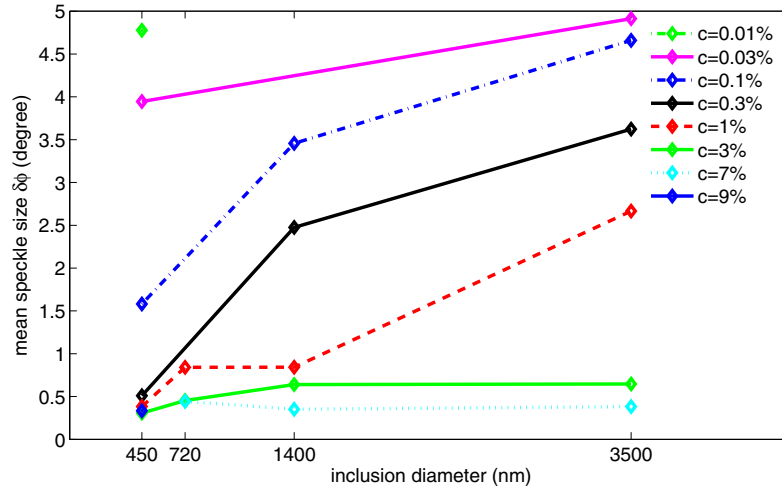


Figure 10. Resultant speckle angle as a function of the inclusion diameter.

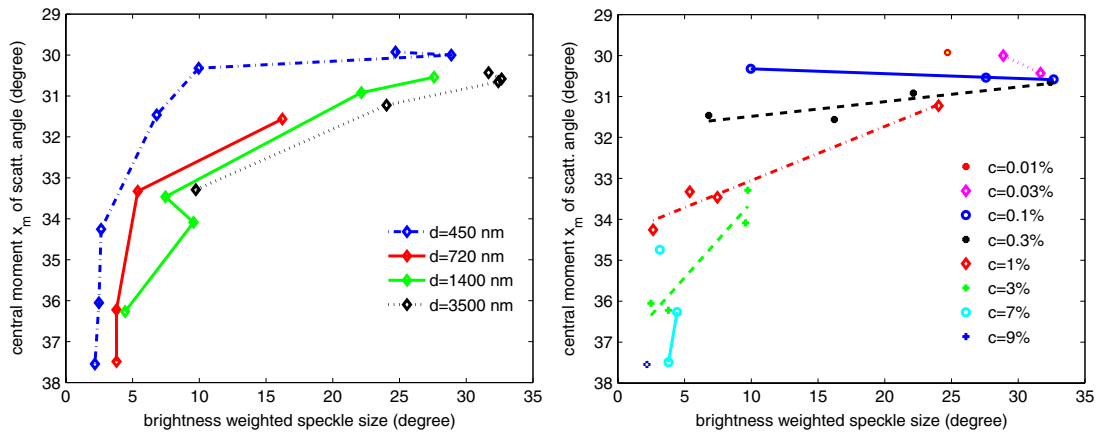


Figure 11. Final result of the combined analysis methods; the results are averaged values, arranged by different diameters (left) and different concentrations (right).

Table 7. Mean values and standard deviations from the speckle analysis (figure 10).

$d$	450 nm	720 nm	1400 nm	3500 nm
$c = 9\%$	$0.334 \pm 0.031$			
$c = 7\%$		$0.443 \pm 0.044$	$0.351 \pm 0.058$	$0.382 \pm 0.087$
$c = 3\%$	$0.307 \pm 0.027$	$0.453 \pm 0.047$	$0.64 \pm 0.24$	$0.646 \pm 0.34$
$c = 1\%$	$0.384 \pm 0.057$	$0.841 \pm 0.55$	$0.843 \pm 0.41$	$2.67 \pm 1.6$
$c = 0.3\%$	$0.51 \pm 0.2$	$3.52 \pm 1.6$	$2.48 \pm 1.4$	$3.62 \pm 1.3$
$c = 0.1\%$	$1.58 \pm 1.1$		$3.46 \pm 1.5$	$4.66 \pm 0.82$
$c = 0.03\%$	$3.95 \pm 1.1$			$4.91 \pm 0.38$
$c = 0.01\%$	$4.78 \pm 0.62$			

hand, our PS particles are produced using potassium peroxide sulfate ( $K_2(SO_4)_2$ ) as an initiator of the polymerization process. Therefore, negative charged  $SO_4$ -groups prevent flocculation or coagulation because of their repulsive force. A net calculation of the total force or potential between two particles using the DLVO theory [21] shows that for water which is slightly impurified by some remainder of the PS polymerization process, there will be only a small (up to about  $3k_B T$ ) or no net attraction between two PS particles. Thus, only minor flocculation will occur within the host droplet due to thermal movements of the particles at the short-time scales of our measurements.

However, we also have to take into account the fluid dynamic properties and the associated movements of the inclusions. An estimation of the fluid velocities during the droplet generation process after Schönfeld *et al* [22] using a jet velocity within the droplet of  $v_{jet} = 1.82 \text{ m s}^{-1}$  leads to kinetic energies of the inclusions of  $E_{kin} = 0.021, 0.086, 0.63, 9.8 \times 10^6 k_B T$  for the inclusion with diameter  $d_{incl} = 450, 720, 1400, 3500 \text{ nm}$ , respectively. These kinetic energies are partly much higher than the repulsive potentials due to surface charge of the inclusions which is about  $\Phi_r < 17000 k_B T$ . So, it is very likely that there are coagulated PS particles within the droplets.

Another very interesting effect is the binding of the PS particles on the surface of the host droplet. Binks *et al* [23] gave a formula for the estimation of the free energy of attachment which yields values of  $\Delta G = 2.7, 6.9, 25.9, 162 \times 10^6 k_B T$ . These energies are even higher than the kinetic energies above and lead, as a consequence, to an irreversible binding of the particles onto the droplet surface.

To mention a last inherent inaccuracy of our data analysis, we want to emphasize that the Mie filtering method does not perfectly filter out the light scattering response of the droplet due to Mie scattering. Hence, the analysed filtered images are more or less noisy which also contributes to increased standard deviations of the evaluation procedure.

Altogether, we assume that the physical properties of the PS particles within the measured droplets are not homogeneous as in dynamic light-scattering experiments because of the jet velocities and the associated probability for flocculation of the particles as well as the tendency to an accumulation of the particles onto the droplet surface. In terms of this viewpoint, the vast standard deviations of the measurements can be explained by the arguments and estimations from above.

## 6. Conclusion

We generated small, nearly monodisperse droplets with inclusions using a piezoelectrical drop-on-demand droplet generator. The droplets were illuminated by monochromatic light and the scattered light intensities were measured with a fast line-scan CCD camera. The captured frames from that camera were analysed by three independent methods. The first method is based on the wavelet transform and yields a measure for the concentration of the inclusions. The second and third methods are the turbidity and the speckle analysis which are combined to give a second parameter extracted from a measurement.

These two parameters serve as an estimation of the inclusion diameter and concentration with the described measurement setup. However, the results are not unique. We explain the large standard deviation of the obtained measurement values by the fact that our evaluation is restricted to 100 measurements, a statistically small sample number. Therefore, only mean values show distinct tendencies regarding different monodisperse inclusion concentrations and diameters. A further reason for the vast standard deviation is the possibility that the inclusions flocculate due to fluid flows within the droplet. Moreover, the light scattered from the droplets will also be influenced by the accumulation of the inclusions onto the droplet surface. We believe that the randomness of flocculation and surface accumulation are responsible for the standard deviation.

To minimize the mentioned flocculation probability, electrostatic or steric stabilized inclusions should be used instead of raw polystyrene latex particles. Moreover, the droplet generation process should be improved to yield more than 100 measurements for one suspension.

## Acknowledgments

The authors acknowledge the support of this research project by the Deutsche Forschungsgemeinschaft (DFG).

## References

- [1] Krieger U K, Corti T and Videen G 2004 Using photon-counting histograms to characterize levitated liquid aerosol particles with a single, solid inclusion *J. Quant. Spectrosc. Radiat. Transfer* **89** 191–200
- [2] Videen G, Ngo D, Chýlek P and Pinnick R G 1995 Light scattering from a sphere with an irregular inclusion *J. Opt. Soc. Am. A* **12** 922–8
- [3] Videen G, Sun W, Fu Q, Secker D R, Greenaway R S, Kaye P H, Hirst E and Bartlex D 2000 Light scattering from deformed droplets and droplets with inclusions: II. Theoretical treatment *Appl. Opt.* **39** 5031–9
- [4] Gouesbet G and Gréhan G 2000 Generalized Lorenz–Mie theory for a sphere with an eccentrically located spherical inclusion *J. Mod. Opt.* **47** 821–37
- [5] Prabhu D R, Davies M and Videen G 2001 Light scattering calculations from oleic-acid droplets with water inclusions *Opt. Exp.* **8** 308–13
- [6] Bronk B V, Smith M J and Arnold S 2000 Photon-correlation spectroscopy for small spherical inclusions in a micrometer-sized electrostatically levitated droplet *J. Aerosol. Sci.* **33** 441–54
- [7] Videen G, Pellegrino P, Ngo D, Nachman P and Pinnick R G 1997 Qualitative light-scattering angular correlations of conglomerate particles *Appl. Opt.* **36** 3532–7
- [8] Jakubczyk D, Derkachov G, Zientara M, Kolwas M and Kolwas K 2000 Local-field resonance in light scattering by a single water droplet with spherical dielectric inclusions *Appl. Opt.* **39** 629–36
- [9] Onofri F, Bergougnoux L, Firpo J-L and Misguich-Ripault J 1999 Size, velocity, and concentration in suspension measurements of spherical droplets and cylindrical jets *Appl. Opt.* **38** 4682–90
- [10] Rheims J, Wriedt T and Bauckhage K 1999 Sizing of inhomogeneous particles by differential laser Doppler anemometer *Meas. Sci. Technol.* **10** 68–75
- [11] Wriedt T and Schuh R 2002 The inclusion-concentration measurement of suspension droplets based on Monte Carlo ray tracing *Meas. Sci. Technol.* **13** 276–9
- [12] Schuh R, Riefler N and Wriedt T Sizing of single inhomogeneous droplets with high inclusion concentration by investigating the scattered speckle field, to be published
- [13] Ulmke H, Wriedt T, Lohner H and Bauckhage K 1999 The piezoelectric droplet generator; a versatile tool for dispensing applications and calibration of particle sizing instruments *Precision Engineering—Nanotechnology: Proc. 1st Int. Euspen Conf.* P McKeown *et al* (Aachen: Shaker) pp 290–3
- [14] Frohn A and Roth N 2000 *Dynamics of Droplets* (Berlin: Springer)
- [15] Hubbard B B 1996 *The World According to Wavelets* (Wellesley: Peters)
- [16] Kaiser G A *Friendly Guide to Wavelets* (Boston, MA: Birkhäuser)
- [17] Pratt W K 2001 *Digital Image Processing* (New York: Wiley)
- [18] Gonzalez R C and Woods R E 2002 *Digital Image Processing* (Englewood Cliffs, NJ: Prentice-Hall)
- [19] Xu R 2000 *Particle Characterization: Light Scattering Methods* (Dordrecht: Kluwer)
- [20] Goodman J W 1975 Statistical properties of laser speckle patterns *Laser Speckle and Related Phenomena* ed J C Dainty (Berlin: Springer) pp 9–77
- [21] Hiemenz P C and Rajagopalan R 1997 *Principles of Colloid and Surface Chemistry* (New York: Dekker)
- [22] Schönfeld F and Rensink D 2003 Simulation of droplet generation by mixing nozzles *Chem. Eng. Technol.* **26** 585–91
- [23] Binks B P and Horozov T S 2006 *Colloidal Particles at Liquid Interfaces* (Cambridge: Cambridge University Press)